ACS APPLIED MATERIALS & INTERFACES

Research Article

www.acsami.org

Ultrathin Ammonium Heptamolybdate Films as Efficient Room-Temperature Hole Transport Layers for Organic Solar Cells

Weiming Qiu,*[,†,‡] Afshin Hadipour,[†] Robert Müller,[†] Bert Conings,[∥] Hans-Gerd Boyen,[∥] Paul Heremans,[†,§] and Ludo Froyen[†,‡]

[†]Imec, Kapeldreef 75, 3001 Heverlee, Belgium

[‡]Department of Metallurgy and Materials Engineering, KU Leuven, 3001 Heverlee, Belgium

[§]Department of Electrical Engineering (ESAT), KU Leuven, 3000 Heverlee, Belgium

[∥]University of Hasselt, Wetenschapspark 1, 3590 Diepenbeek, Belgium

Supporting Information

ABSTRACT: Ammonium heptamolybdate $(NH_4)_6Mo_7O_{24}\cdot 4H_2O$ (AHM) and its peroxo derivatives are analyzed as solution-processed room temperature hole transport layer (HTL) in organic solar cells. Such AHM based HTLs are investigated in devices with three different types of active layers, i.e., solution-processed poly(3-hexylthiophene)/[6,6]-phenyl C_{61}-butyric acid methyl ester(P3HT/PC_{60}BM), poly[*N*-9′-heptadecanyl-2,7-carbazole-*alt*-5,5-(4′,7′-di-2-thienyl-2′,1′,3′-benzothiadiazole)]/[6,6]-phenyl C_{70}-butyric acid methyl ester-(PCDTBT/PC_{70}BM) and evaporated small molecule chloro-(subphthalocyaninato)boron(III) (SubPc)/C_{60}. By virtue of their high work functions, AHM based HTLs outperform the commonly used poly(3,4-ethylenedioxythiophene):polystyrenesulfonate (PEDOT:PSS) HTL for devices employing deep HOMO level active materials. Moreover, devices using AHM based HTLs can achieve higher short circuit current (J_{sc}) than the ones with evaporated molybdenum oxide($eMoO_3$), and thus better power conversion efficiency (PCE). In addition, P3HT/PC_{60}BM devices with AHM based HTLs show air stability comparable to those with $eMoO_3$, and much better than the ones with PEDOT:PSS.

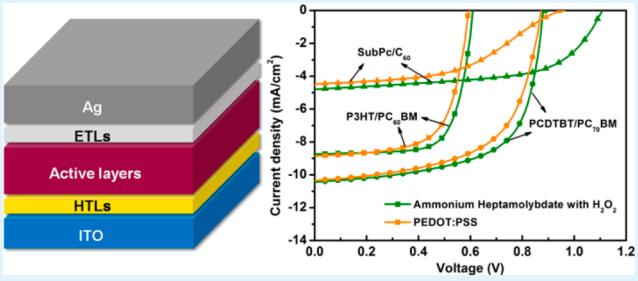

KEYWORDS: *ammonium heptamolybdate, H_2O_2 modification, room temperature, hole transport layers, organic solar cells*

1. INTRODUCTION

Organic solar cells have become a promising alternative technology for producing clean and renewable energy by virtue of their unique advantages, such as low-cost, simple manufacturing process, flexibility and low weight.[1−3] So far, the power conversion efficiency (PCE) of state-of-the-art organic solar cells has already passed 10%, which is a huge step toward practical applications.[4] To design efficient and stable organic solar cells, one of the critical aspects is the interface engineering between the active layer and the electrodes. Usually, indium tin oxide (ITO) and silver (Ag) are used as transparent and reflective electrodes, respectively. However, none of those electrodes has the proper interface with the photoactive layer. To extract charges in an efficient way, buffer layers are required between photoactive layers and electrodes of the devices. For example, ZnO and TiO_2 are frequently used as electron transport layers, while poly(3,4-ethylenedioxythiophene):polystyrenesulfonate (PEDOT:PSS) and MoO_3 are typical hole transport materials, to extract electrons and holes, respectively.[5,6] Such buffer layers have the function of tuning the energy level alignment at the electrode/photoactive layer interface to form an ohmic contact, improving charge selectivity for corresponding electrodes, and are also associated tightly with the device stability.[7−10]

PEDOT:PSS is presently the most commonly used hole transport layer (HTL) material, due to its good electrical properties and great solution processability. However, it has also been pointed out that the high acidity and hygroscopic nature of PEDOT:PSS have detrimental effects on the long-term stability of organic solar cells.[11,12] Therefore, PEDOT:PSS is not suitable as the ultimate interface modification material for stable organic solar cell technologies. Moreover, for polymer donors with very deep highest occupied molecular orbit (HOMO) levels, the work function of PEDOT:PSS (5.1 eV) is not high enough to efficiently extract the holes, resulting in the lowering of the open circuit voltage (V_{oc}), FF and thus the decreasing of the PCE.[13]

With the aim to replace PEDOT:PSS; solution processable high work function transition metal oxides (TMOs), such as MoO_3, V_2O_5, NiO, and WO_3, have been widely investigated as HTL materials.[14−18] This is due to their favorable band

Received: July 14, 2014
Accepted: August 29, 2014
Published: August 29, 2014

structures, excellent stability in the ambient environment and compatibility with large-area solution processing technologies. By employing such metal oxide for HTLs, devices with comparable efficiency but increased stability over the PEDOT:PSS based ones have been reported.[19−21] Nevertheless, to make these TMO layers, high annealing temperatures are normally required to convert the precursors into high quality metal oxides in most cases.[21−24] For example, molybdenum oxide based HTLs made by dissolving MoO_3 powder in hydrogen peroxide needed to be annealed at a temperature of 275 °C in air to provide good hole extraction and transport properties for organic solar cells.[22] Such high temperatures are, however, incompatible with low-cost flexible plastic substrates used for large-scale production. To solve this problem, sol−gel processed metal oxide HTLs with annealing temperatures below 150 °C (compatible with low-cost flexible substrates) have been reported recently, but the preparation procedures are often time-consuming or proved to require treatments such as UV-ozone.[25−27] Another approach to overcome this problem is the application of spin-coated HTL layers from colloidal TMO nanoparticle solutions. However, significant roughness and pinholes may be observed in such films.[28] Moreover, additional treatments, for example oxygen-plasma, are required after spin-coating to remove the dispersing agents in order to improve the electrical properties.[29,30] As a result, facile and effective ways of fabricating HTLs that can replace PEDOT:PSS in organic solar cells are still highly desired.

Ammonium heptamolybdate ($(NH_4)_6Mo_7O_{24}\cdot 4H_2O$) (AHM) is a commercially available reagent, used for instance in the preparation of MoO_3 from solution. It was first introduced by Liu et al. for solution processed molybdenum oxide (s-MoO_x) thin films in organic solar cell application.[31] In their recipe, hydrochloric acid addition is required in the s-MoO_x preparation, as well as a thermal annealing step at 160 °C in nitrogen after spin-coating. The aggregation of s-MoO_x resulted in a reduced film uniformity and a lower device performance than for PEDOT:PSS based reference cells. Afterward, Yang's group reported the thermal decomposition of AHM aqueous solution into MoO_3 upon heating at 80 °C for 1 h.[32] AHM was decomposed into three components, i.e., MoO_3, NH_3 and H_2O, among which MoO_3 was the only expected solute in the solution.[32] By using this recipe, the quality of the s-MoO_x layers was significantly improved, and organic solar cell devices that have comparable performance to PEDOT:PSS based devices were achieved. Zhang et al. then reported the in situ formation of MoO_3 using AHM as a precursor in a PEDOT:PSS matrix to produce a smooth and less hygroscopic HTL.[33] Another strategy to fabricate s-MoO_3 film from AHM was developed by Yao et al. using a self-energy generating combustion reaction, which employed acetylacetone and nitric acid (HNO_3) as the fuel and oxidizer, respectively.[34] However, when the annealing temperature is reduced from 250 to 150 °C, a small amount of PEDOT:PSS had to be added to the precursor solution in order to reach sufficient conductivity. Furthermore, the addition of different kinds of reagents apparently makes the recipe more complex. More recently, Chen et al. reported highly dispersed MoO_3 made from AHM by adding dispersant to the solution and then cleaning with nitric acid and anhydrous ethanol under ultrasonic treatment.[35]

In the above-mentioned cases using AHM, it is postulated that its chemical transformation into MoO_3 is necessary to use the material as HTL in organic solar cells. In this paper, we put a new insight into this material, showing that an extremely thin layer of AHM can be used directly as the HTLs for organic solar cells, with very beneficial effects compared to evaporated MoO_3 layers as well as with respect to PEDOT:PSS. Furthermore, instead of converting AHM to MoO_3, we modified it with hydrogen peroxide (H_2O_2), which is reported to increase the stability of the AHM solution.[36] Slightly higher work function and also better device performance can be achieved by using HTLs fabricated from H_2O_2 modified AHM solutions than from pure AHM solutions. Moreover, although solution processed metal oxide HTLs are frequently reported for devices using shallow HOMO level materials like P3HT, their applications in devices employing deep HOMO level materials like PCDTBT are very scarce.[13,37,38] Especially, there are even more limited reports on solution processed HTLs, which can be processed at room temperature without further treatments, for materials with deep HOMO levels. Here, we demonstrated solution processed room temperature AHM based HTLs can outperform PEDOT:PSS and their evaporated metal oxide counterparts for devices using materials with deep HOMO levels. In addition, P3HT/PC_{60}BM devices with the AHM based HTLs show device stability in air comparable with eMoO_3, which itself exceeds that of PEDOT:PSS devices.

2. RESULTS AND DISCUSSION

2.1. Characterization of AHM based HTLs. To gain insight into spin-coated AHM as a HTL layer and its modifications when treated at different temperatures and with auxiliary reagents such as H_2O_2, we carried out analysis with Fourier transform infrared spectroscopy (FT-IR), X-ray photoelectron spectroscopy (XPS), ultraviolet−visible (UV−vis) absorption spectroscopy, atomic force microscopy (AFM) and also contact angle measurements.

The FT-IR spectra of the AHM films before and after annealing are illustrated in Figure 1a. As-prepared and 110 °C treated AHM films show almost identical FT-IR spectra compared to the AHM powder. These peaks are also consistent with the literature: the peak around 3511 cm^{-1} and the multiple

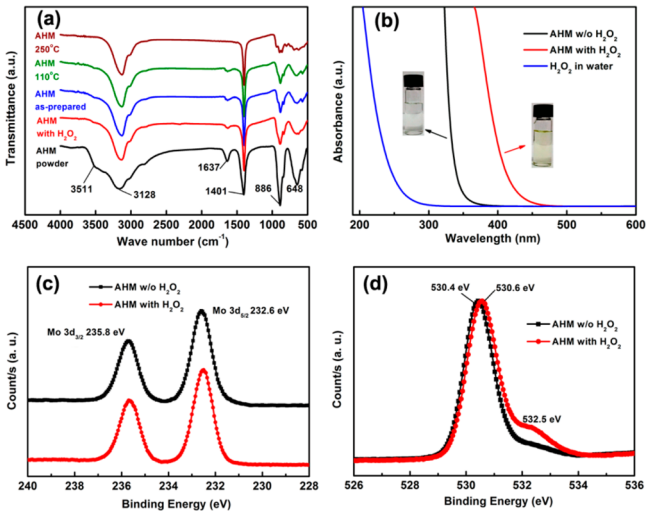

Figure 1. (a) FT-IR spectra of AHM powder and AHM based films; (b) UV−vis spectra of pure AHM solution, AHM solution with H_2O_2 treatment, and H_2O_2 in water; (c) Mo 3d core level XPS spectra of AHM without H_2O_2 and AHM with H_2O_2; (d) O 1s core level XPS spectra of AHM without H_2O_2 and AHM with H_2O_2.

peaks around 3128 cm^{-1} represent the stretching modes of H_2O and NH_4^+, which are hydrogen bridging to the terminal oxygen of the Mo−O octahedral; the peaks at 1637 and at 1401 cm^{-1} are attributed to H_2O and NH_4^+ bending mode.[39] After annealing at 250 °C, the peaks at 3511 and 1637 cm^{-1} disappear, implying the loss of structural water. However, the peaks for NH_4^+ remained unchanged. The above facts show that the obtained AHM films have excellent thermal stability and even baking them at 110 °C does not change their chemical composition. Moreover, for the HTL layer prepared from the solution with H_2O_2 as additive (noted as AHM with H_2O_2 below), no obvious difference was observed in the FI-IR spectra with respect to that obtained from pure AHM solution, indicating they have similar chemical composition. These findings were confirmed by XPS survey scans, showing no measurable difference between pristine and annealed films, neither between films with and without H_2O_2 modification (see Figure S1, Supporting Information). The N:Mo ratios in the films without and with H_2O_2 modification were determined to be 0.89 and 0.87, respectively. Within the error of the measurement, this corresponds to a theoretical value of 0.86.

UV−vis absorption measurements were carried out on AHM solutions without and with H_2O_2 addition. As is clearly shown in Figure 1b, by adding H_2O_2 to an AHM solution, the absorption onset of the solution shifts to longer wavelengths, leading to a color change from transparent to light yellow. The optical band gaps of AHM solution without and with H_2O_2 modification can be obtained from the Tauc plot,[40] and a reduction of optical band gap from 3.75 to 3.17 eV is observed after H_2O_2 modification (Figure S2, Supporting Information). Such a decrease of optical band gap apparently implies the change of solution composition before and after the adding of H_2O_2 due to the interaction between H_2O_2 and AHM, though the above FT-IR measurements and XPS survey scan show that both solutions might still have very similar composition. It has been reported that peroxo derivatives of polymolybdates are formed when the polymolybdates are reacted with H_2O_2:[41]

$$Mo_7O_{24}^- + 2H_2O_2 \rightarrow Mo_7O_{22}(OO)_2^- + 2H_2O \quad (1)$$

Therefore, it is reasonable to assume that peroxidation reaction of AHM will also occur during H_2O_2 treatment in our case, which results in a slight change of its chemical composition. In addition, the pH value of the solution decreased slightly from 5.06 to 4.86 after the addition of H_2O_2, which is consistent with the literature report and probably because of the increased number of electronegative O atoms in the AHM peroxo derivates.[41] To deepen the understanding of the effects of H_2O_2 treatment, XPS core level measurements were also performed on the films obtained from solutions with and without H_2O_2. Seen from the Mo 3d core level spectrum (Figure 1c), both the AHM film and AHM with H_2O_2 film show a Mo $3d_{5/2}$ peak of 232.6 eV and a Mo $3d_{3/2}$ peak of 235.8, which are consistent with the values reported for AHM.[42] Therefore, the addition of H_2O_2, which is a strong oxidizer, does not change the oxidation state of molybdenum species, which is Mo^{6+} in both films. In the O 1s spectra (Figure 1d), the main peaks at 530.4 and 530.6 eV are observed for AHM and AHM with H_2O_2 films, respectively, which coincide within the error margin of the measurement with the typical binding energy of O 1s in a transition metal−oxygen (TM-O) bond around 530.5 eV and the oxygen species integrated in the material as O_2^{2-}, having binding energies in the range of 530.5 to 531.1 eV.[43] However, an enhanced peak around 532.5 eV, which can be assigned to the structural water,[43,44] is found for the AHM with H_2O_2 film, probably indicating the increase of structural water in the peroxoderivates of AHM. On the basis of all the characterization methods, it can be concluded that AHM does not transform to MoO_3 in our recipe, whereas H_2O_2 modification leads to the formation of peroxo derivates of AHM with narrower band gap than AHM.

To investigate the surface morphology of corresponding films on ITO substrates, tapping mode AFM images of the AHM based HTLs without and with H_2O_2 modification are given in Figure 2a,c using a 4 × 4 μm scan size. The films

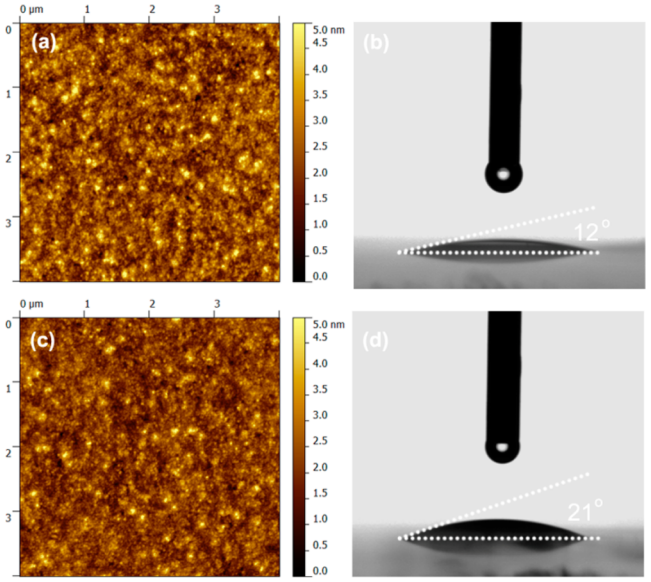

Figure 2. AFM and contact angle images showing the surface properties of the films spin coated from AHM solution (a, b) and AHM solution with H_2O_2(c, d).

prepared by directly spin-coating AHM and H_2O_2 modified AHM solutions have a very smooth surface morphology with root-mean-square (RMS) roughness values of 0.72 and 0.61 nm respectively, which are lower than the HTLs made from MoO_3 solutions using solely AHM as a precursor.[31,32] The RMS values are also considerably lower than those of s-MoO_3 prepared from nanoparticle suspensions (15−30 nm).[28] Clearly, by virtue of their high smoothness and homogeneity, our films are very promising as HTLs of organic solar cell devices. Static contact angle measurement is also used to evaluate the surface properties of the AHM based layers, using deionized water as the solvent. The contact angles for the films made from AHM solution and AHM with H_2O_2 solution are 12° and 21°, respectively, indicating a slightly difference in surface energy between them (Figure 2b,d).

2.2. Device Performance. The work functions of the HTLs are crucial to their performance when used in organic solar cell devices. For efficient hole extraction, their work function should be high enough to pin the Fermi level to the positive integer charge-transfer state of the donor materials, according to the integer charge-transfer (ICT) model.[45] Therefore, the work functions of the AHM based HTLs on ITO substrates were measured by ultraviolet photoelectron spectroscopy (UPS), using bare ITO substrates and ITO/PEDOT:PSS as a reference. Calculated from the second electron cutoff of the curves shown in Figure 3, the work functions of bare ITO and ITO/PEDOT:PSS are 4.83 and 5.20

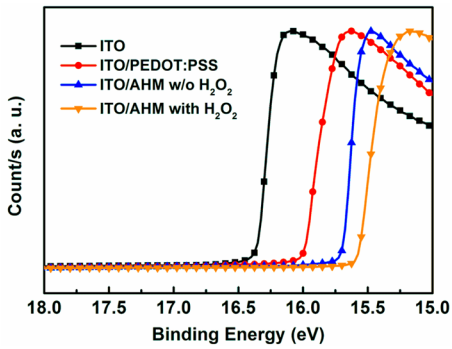

Figure 3. UPS spectra of bare ITO and ITO deposited with different HTLs. The HTLs are processed using the same methods for device fabrication.

eV, respectively, which are close to their reported values.[13] ITO/AHM w/o H_2O_2 gives a higher work function of 5.50 eV than PEDOT:PSS. Remarkably, by adding H_2O_2 to AHM solution before spin-coating, the work function of the obtained film (ITO/AHM with H_2O_2) can further increase to 5.62 eV. Such high work functions of our AHM based layers indicate their possibility as high performance HTLs for organic solar cells.

To demonstrate the effectiveness of our AHM based HTLs, three types of organic solar cell devices were made in this study, with the HOMO level of the donor materials decrease from −4.76 eV (P3HT),[21] −5.45 eV (PCDTBT),[13] to −5.6 eV (SubPc).[46] The chemical structures of the organic materials used in different devices are illustrated in Figure 4a. AHM based HTLs were spin coated from 0.4 wt % AHM solutions without and with H_2O_2 modification, resulting in the optimized thickness of around 4 nm for this solution processed layer, as will be shown below. The benchmark HTLs, i.e., 25 nm PEDOT:PSS and 10 nm eMoO_3 were used for comparison.

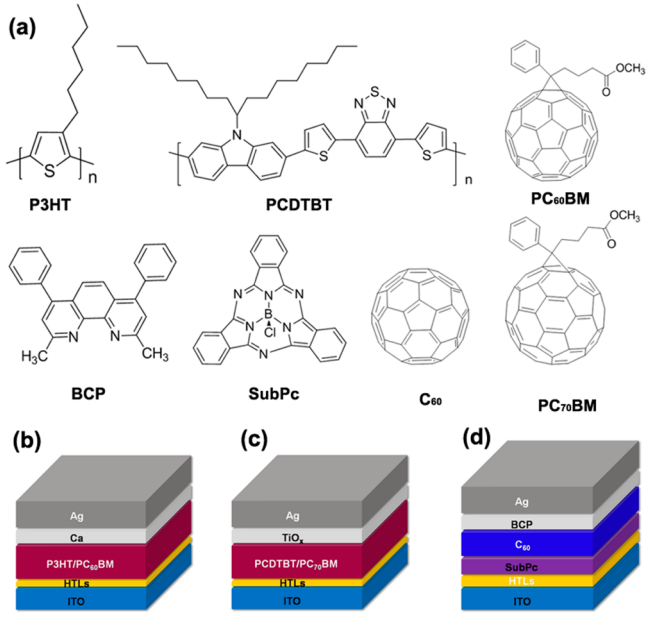

Figure 4. (a) Chemical structures of the organic materials used in different devices; (b) scheme of the P3HT/$PC_{60}BM$ device structure; (c) scheme of the PCDTBT/$PC_{70}BM$ device structure; (d) scheme of the SubPc/C_{60} device structure.

The detailed processing recipes are described in the Experimental Section.

P3HT/$PC_{60}BM$ devices, with the structure ITO/HTLs/P3HT: $PC_{60}BM$/Ca/Ag (Figure 4b), were first fabricated and characterized. The typical photocurrent density−voltage (J−V) and external quantum efficiency (EQE) curves of such devices using different HTLs are shown in Figure 5a,b, respectively. The average performance of 12 devices is also summarized in Table 1. Clearly, the devices using our AHM based HTLs have comparable performance to those using the benchmark HTLs. We also find almost no difference on device performance is observed between devices with and without baking (Figure S3, Supporting Information). Therefore, our AHM based HTLs can be prepared simply at room temperature and work efficiently without any thermal or other treatments after deposition. It is also noteworthy that because the work function of PEDOT:PSS is sufficiently high compared to the HOMO level of P3HT, similar V_{oc} and PCE values are observed between the PEDOT:PSS based and AHM based devices, which is consistent with the previous report.[47] Moreover, a slight difference in photovoltaic parameters is observed between the devices using AHM with and without H_2O_2 HTLs. Recently, Tremolet de Villers and co-workers reported that the solution processed MoO_x HTLs obtained from different annealing temperatures could induce very different vertical distribution in P3HT/$PC_{60}BM$ layers, and the accumulation of $PC_{60}BM$ near the HTL surface greatly reduced the FF.[48] This means the surface properties of the HTL have influence on the morphology of the active layer. In our case, it is possible that the difference in surface properties between pure AHM and modified AHM films, indicated by AFM and contact angle measurements, may also influence the phase separation and vertical distribution of the active layer. Therefore, we assume the higher FF of the devices using AHM with H_2O_2 HTL is probably due to the favored active layer morphology for charge extraction. However, it is difficult to establish its exact origins, since the improvement is not significant.

Interestingly, the above results are in contradiction with previous reports mentioning that pristine AHM layers could not play the role of efficient HTLs to improve the performance of organic solar cell devices, though an increased work function was also measured when depositing an AHM layer on ITO.[38,49] In the study conducted by Griffin et al.,[38] spray coated AHM films needed to be annealed at 350 °C in order to provide good hole transport properties. During this treatment, the film thickness diminished from 13.2 to 7.7 nm, and the decrease of series resistance was also observed. Therefore, we assume that the reason for the low performance of pristine AHM based devices reported in literature is the use of too thick of AHM layers. To verify our assumption, the dependence of P3HT/$PC_{60}BM$ device performance on the HTL thickness is investigated on devices using AHM with H_2O_2 HTLs. HTL thickness was varied by changing the AHM concentration in solution and measured by ellipsometry. With the same processing conditions (spin speed), if the AHM concentration increases from 0.4 to 1.6 wt %, the thickness of the film increases from around 4 to near 16 nm correspondingly (Figure S4, Supporting Information). The J−V curves of the devices using H_2O_2 modified AHM HTLs with different thickness are illustrated in Figure 5c,d. From the curves recorded under illumination (Figure 5c), it can be found that J_{sc} and V_{oc} do not change significantly with HTL thickness. However, the FF and

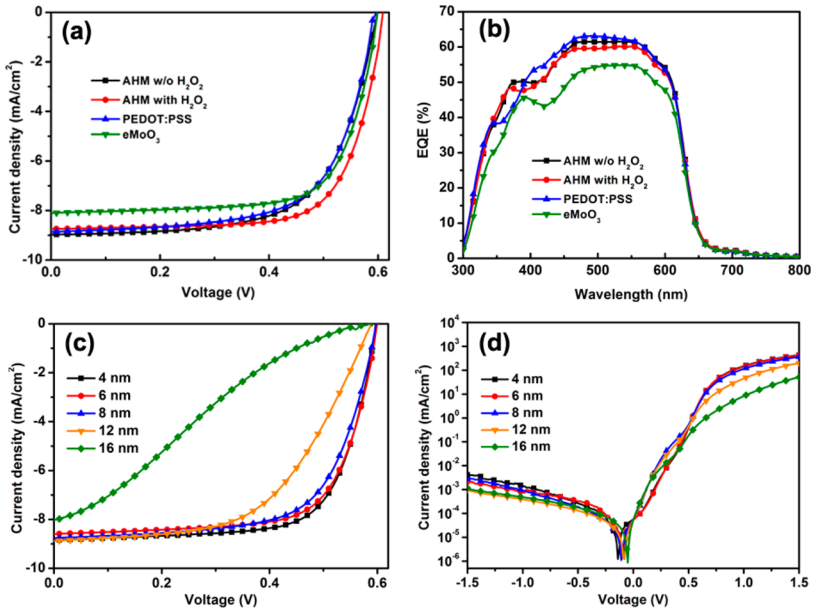

Figure 5. (a) Light $J-V$ curves of P3HT/PC_{60}BM devices using different HTLs; (b) EQE curves of P3HT/PC_{60}BM devices using different HTLs; (c) light $J-V$ curves of P3HT/PC_{60}BM devices using HTLs fabricated from H_2O_2 modified AHM solution with different thicknesses; (d) dark $J-V$ curves of P3HT/PC_{60}BM devices using HTLs fabricated from H_2O_2 modified AHM solution with different thicknesses. The phenomenon that the lowest points of dark curves shift to negative bias is due to the capacitive errors in the measurement setup when measuring very low currents.

Table 1. Detailed Average Photovoltaic Parameters of P3HT/PC_{60}BM Devices Using Different HTLs[a]

HTLs	J_{sc} (mA/cm^2)	V_{oc} (V)	FF (%)	PCE (%)
AHM w/o H_2O_2	8.85 ± 0.12	0.60 ± 0.00	64.61 ± 1.13	3.39 ± 0.06
AHM with H_2O_2	8.75 ± 0.08	0.61 ± 0.00	69.83 ± 1.24	3.76 ± 0.07
PEDOT:PSS	8.85 ± 0.08	0.61 ± 0.01	64.91 ± 1.52	3.53 ± 0.08
$eMoO_3$	8.05 ± 0.05	0.60 ± 0.01	69.39 ± 1.02	3.40 ± 0.07

[a]Results are expressed as mean value ± standard deviation from 12 devices.

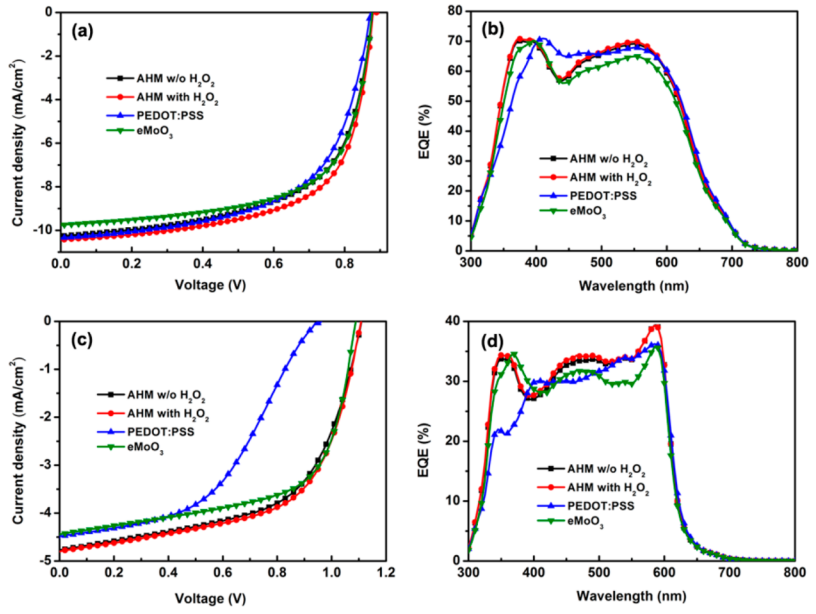

Figure 6. (a) Light $J-V$ curves of PCDTBT/PC_{70}BM devices using different HTLs; (b) EQE curves of PCDTBT/PC_{70}BM devices using different HTLs; (c) light $J-V$ curves of SubPc/C_{60} devices using different HTLs; (d) EQE curves of SubPc/C_{60} devices using different HTLs.

therefore also the PCEs of the devices drastically decrease when the HTL thickness is above 10 nm. Moreover, an S-shaped curve is observed if the thickness is around 16 nm due to the inefficient extraction of holes.[50] From the dark curves of the corresponding devices, the forward biased current density at high voltage decreases toward the increase of film thickness (Figure 5d), indicating the increase of series resistance with film thickness of AHM based HTLs. These findings are consistent

Table 2. Detailed Average Photovoltaic Parameters of PCDTBT/$PC_{70}BM$ Devices Using Different HTLs[a]

HTLs	J_{sc} (mA/cm^2)	V_{oc} (V)	FF (%)	PCE (%)
AHM w/o H_2O_2	10.20 ± 0.04	0.88 ± 0.01	61.46 ± 0.98	5.48 ± 0.10
AHM with H_2O_2	10.36 ± 0.07	0.88 ± 0.01	63.23 ± 0.45	5.73 ± 0.08
PEDOT:PSS	10.29 ± 0.06	0.86 ± 0.01	58.40 ± 1.12	5.21 ± 0.12
$eMoO_3$	9.83 ± 0.04	0.88 ± 0.01	63.26 ± 0.86	5.42 ± 0.11

[a]Results are expressed as mean value ± standard deviation from 12 devices.

Table 3. Detailed Average Photovoltaic Parameters of SubPc/C_{60} Devices Using Different HTLs[a]

HTLs	J_{sc} (mA/cm^2)	V_{oc} (V)	FF (%)	PCE (%)
AHM w/o H_2O_2	4.75 ± 0.04	1.11 ± 0.01	57.23 ± 0.54	3.03 ± 0.03
AHM with H_2O_2	4.78 ± 0.05	1.11 ± 0.00	58.59 ± 0.47	3.11 ± 0.05
PEDOT:PSS	4.49 ± 0.06	0.96 ± 0.01	46.25 ± 0.42	1.99 ± 0.05
$eMoO_3$	4.44 ± 0.04	1.09 ± 0.00	62.18 ± 0.38	3.00 ± 0.03

[a]Results are expressed as mean value ± standard deviation from 12 devices.

with the results reported by Griffin et al. and also our assumption. Therefore, very thin AHM based HTLs are required in order to improve the performance of organic solar cell devices. Under such conditions, they can increase the work function of ITO substrate to facilitate the extraction of holes, while the resistivity of the films stays low.

When donor materials with very deep HOMO levels are used, performance of the devices relies more critically on the properties of the HTLs than P3HT/$PC_{60}BM$ ones.[12,29] So far, there are very limited successful applications of solution processed HTLs in such devices.[8,12,22] Moreover, for all of them, thermal annealing treatments at very high temperatures are needed. To verify further the reliability of our AHM based HTLs for devices using deep HOMO level materials, a solution processed PCDTBT/$PC_{70}BM$ device with TiO_x as the electron transport layer (Figure 4c), and thermally evaporated small molecular SubPc/C_{60} device with bathocuproine (BCP) as the electron transport layer (Figure 4d) were also prepared. The typical $J-V$ and EQE curves are given in Figure 6. The average performance of the PCDTBT/$PC_{70}BM$ devices and the SubPc/C_{60} devices are summarized in Tables 2 and 3, respectively. As shown in Figure 6a and Table 2, for the PCDTBT/$PC_{70}BM$ system, the PEDOT:PSS device exhibits the lowest PCE because of the decreased V_{oc} and FF, which is consistent with the observation of Olson et al. and is resulted from the relatively lower work function of PEDOT:PSS.[13] It is worth noting that our PEDOT:PSS reference devices show relatively lower PCE values (5.21%), compared to the reported value (5.7%) for the similar PEDOT:PSS based PCDTBT/$PC_{70}BM$ devices.[13] This is probably due to the difference in the quality of PCDTBT materials and also in the processing conditions. The inferiority of PEDOT:PSS is more obvious for SubPc/C_{60} system, where an S-shaped $J-V$ curve is recorded (Figure 6c), implying the inefficient extraction of holes when the applied voltage is close to V_{oc}. However, in both material systems, the devices with the AHM based HTLs show optimized V_{oc} and comparable FF to the ones with $eMoO_3$, indicating the formation of good ohmic contact between the donor material and the AHM based HTLs. It is also worth mentioning that the shape of the EQE curve for the device with PEDOT:PSS for the SubPc/C_{60} device differs from the AHM based devices in the range from 350 to 400 nm. This is due to the difference in optical interference effects that related to the HTL thicknesses.

The contact properties between the HTLs and the active layers are also reflected by series resistances. The series resistances of the devices shown in Figures 5a and 6a,c are summarized in Table 4. For the P3HT/$PC_{60}BM$ system, the

Table 4. Series Resistances Calculated from the Inverse Slope of the $J-V$ Curves at 1.5 V for the Devices Shown in Figure 5a and 6a,c, Respectively

	Series Resistance (Ω·cm^2)		
HTLs	P3HT/$PC_{60}BM$	PCDTBT/$PC_{70}BM$	SubPc/C_{60}
AHM w/o H_2O_2	1.8	1.5	6.07
AHM with H_2O_2	1.5	1.3	5.22
PEDOT:PSS	2.4	2.9	5443
$eMoO_3$	1.6	1.6	3.64

series resistances of all the devices are very low and at the same level, indicating the formation of good ohmic contact at the interfaces for all the HTLs. For the PCDTBT/$PC_{70}BM$ system, the series resistances of the devices using AHM based HTLs and $eMoO_3$ are still comparable. However, the PEDOT:PSS devices show higher series resistances than these with the other three types of HTLs, which could be probably attributed to the mismatch between the work function of PEDOT:PSS and the HOMO level of PCDTBT. This becomes much more obvious when SubPc is chosen as the donor material. The SubPc/C_{60} device with PEDOT:PSS has a series resistance of 5443 Ω·cm^2, which is 3 orders larger than that of the devices with AHM based HTLs and $eMoO_3$. Such a high series resistance implies a nonohmic contact between PEDOT:PSS and SubPc. Moreover, a clear relation between the work functions of the HTLs and the magnitudes of series resistances can be observed in the SubPc/C_{60} devices, showing that a higher work function of the HTL leads to a lower series resistance. Thus, in our case, better ohmic contact between the HTL and the active layer can be formed by using AHM with H_2O_2 layer compared to pure AHM layer.

All the above results confirm that our solution processed AHM based HTLs can work efficiently for devices with different HOMO levels. In the case of devices with deep HOMO donor materials, superior performance can be achieved by using AHM based HTLs instead of PEDOT:PSS. Moreover, by comparing the J_{sc} of devices using AHM based HTLs and $eMoO_3$, the $eMoO_3$ devices have lower J_{sc} values in all three types of devices we tested here, which can also be verified by the EQE curves. The higher J_{sc} enables the devices with AHM based HTLs to outperform the ones with $eMoO_3$ in terms of

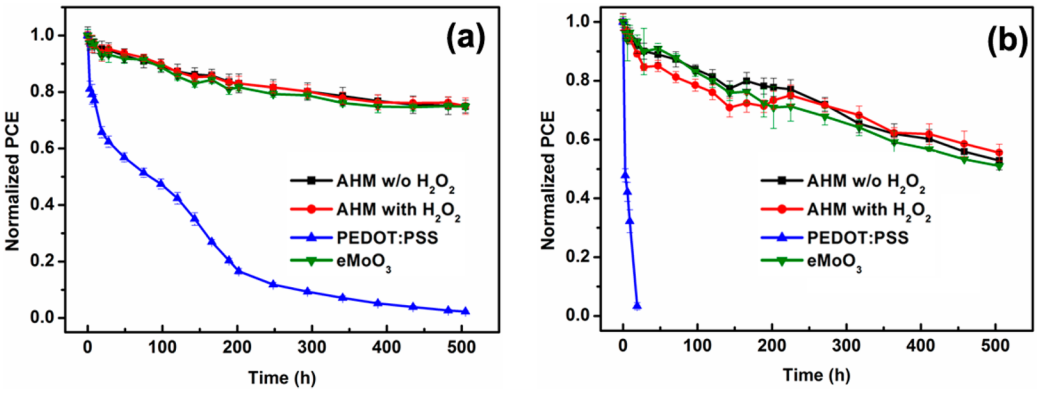

Figure 7. Normalized PCEs of P3HT:$PC_{60}BM$ conventional devices as a function of storage time in air at humidity level of (a) 45% and (b) 75%. The error bars represent the standard deviation for 12 devices.

PCEs. As has been reported in our previous work, reflection losses at the ITO/MoO_3 interface, due to high reflection index of MoO_3, is the main reason for the reduced J_{sc} value when $eMoO_3$ is used as a HTL in conventional devices.[5] Moreover, due to the difference in thicknesses of AHM based HTLs and $eMoO_3$, for the devices using very thin active layers like PCDTBT/$PC_{70}BM$ (70 nm) and SubPc/C_{60} (50 nm), the influence of optical interference also need to be taken into account, which explains the change in the shape of EQE curves for the devices using HTLs with different thicknesses.

2.3. Air Stability Tests. With Ca/Ag as the top contact, the air stability of P3HT:$PC_{60}BM$ conventional structure devices using our AHM based HTLs are compared to these with PEDOT:PSS and $eMoO_3$. To study the influence of humidity on the stability of devices using such water based AHM and H_2O_2 modified AHM HTLs, two sets of devices are kept in air with 45% and 75% humidity, respectively. All the devices are stored without encapsulation. The degradation trends of PCEs, J_{sc}, V_{oc} and FF over storage time are shown in Figures 7 and S5 (Supporting Information). For the devices with PEDOT:PSS, a fast degradation can already be observed upon storage in 45% humidity. Moreover, humidity has significant influence on the stability of PEDOT:PSS devices. As is shown in Figure 7b, storage in 75% humidity accelerates the degradation of the PEDOT:PSS devices severely and they can therefore only survive for a few hours. The above observations are consistent with the results reported by Voroshazi et al.[12] The ambient humidity attracted by the hygroscopic PEDOT:PSS will diffuse toward the highly reactive metal cathode, i.e., Ca in this case, leading to the rapid oxidation of the cathode and result in the increase of series resistance, which explains the decrease of J_{sc} and FF. When $eMoO_3$ is employed as HTL instead of PEDOT:PSS, the device stability is greatly improved, because the above-mentioned degradation mechanism does not take place because $eMoO_3$ is not hygroscopic. The devices using our AHM based HTLs, both with and without H_2O_2 treatment, exhibit almost identical stability with those using $eMoO_3$, keeping 80% of the PCEs after storage in 45% and 75% humidity for around 300 and 130 h, respectively. Although our AHM based HTLs are water-soluble and prepared from aqueous solution, the above observations indicate they are neither significantly hygroscopic nor degraded by humidity. Therefore, such AHM based films are very promising interfacial layers for organic solar cells in terms of long-term stability.

3. CONCLUSIONS

In summary, in contrast to previous reports, we have demonstrated that very thin AHM based films can serve as effective hole transport buffer layers for organic optoelectronic devices like organic solar cells, without any thermal treatment before or after film deposition. Such AHM based HTLs are demonstrated to work for organic solar cells using donor materials with different HOMO levels. In the case of devices employing donor materials with very deep HOMO levels, superior performance can be achieved by using our AHM based HTLs instead of PEDOT:PSS. To the best of our knowledge, this is also the first report of solution processed room temperature HTLs having high enough work function for devices using donor materials with HOMO level as deep as −5.6 eV. In addition, in terms of device stability, the devices with solution processed AHM based layers exhibit significantly better long-term stability compared to those using PEDOT:PSS. Therefore, these AHM based HTLs are promising alternatives to PEDOT:PSS for producing low-cost, large scale and high efficiency organic solar cells.

4. EXPERIMENTAL SECTION

4.1. Device Fabrication. The patterned ITO substrates were first cleaned with detergent, and then ultrasonicated in deionized water, acetone, and isopropyl alcohol for 10 min, respectively. Subsequently, UV-ozone treatment was used to clean the ITO substrates further and to improve the wetting ability for aqueous solutions. Different concentrations of AHM solutions were prepared by dissolving desired amounts of AHM powder (99.99% purity, Aldrich) in deionized water. To make an H_2O_2 modified solution, 10 μL of 30% H_2O_2 was added into 10 mL of 0.4 wt % AHM solution (a [H_2O_2]:[AHM] molar ratio of 3:1). The color of the solution changed from transparent to light yellow immediately. Afterward, the AHM solutions with and without H_2O_2 were spin-coated on the precleaned ITO substrates at 2000 rpm for 60 s to make the solution-processed AHM based HTLs. For comparison, 25 nm spin-coated PEDOT:PSS (Heraeus Clevios 4083) or 10 nm evaporated MoO_3 were also deposited on the ITO as the HTLs. The AHM and PEDOT:PSSHTLs were baked at 110 °C inside a nitrogen filled glovebox in order to drive out the residual water. For the P3HT/$PC_{60}BM$ devices, the *ortho*-dichlorobenzene solution of P3HT and $PC_{60}BM$ (1:0.8 weight ratio) was spin-coated on different HTLs to form the active layer with a thickness of 200 nm, and then annealed at 130 °C for 10 min inside the nitrogen filled glovebox. Finally, 20 nm of Ca and 150 nm of Ag were evaporated onto the active layers subsequently through a shadow mask defining twelve 0.13 cm^2 area devices on one substrate. For the PCDTBT/$PC_{70}BM$ devices, the *ortho*-dichlorobenzene solution of PCDTBT and $PC_{70}BM$ (1:4 weight ratio) was spin coated on different HTLs to form the

active layer with a thickness around 70 nm, and then annealed at 70 °C for 10 min inside the nitrogen filled glovebox. After this, a sol−gel prepared TiO_x solution was spin coated on the active layer with a recipe reported previously.[6] The devices are completed by depositing 150 nm Ag onto the TiO_x through shadow masks. For the SubPc/C_{60} devices, 15 nm SubPc, 35 nm C_{60}, 10 nm BCP and 120 nm Ag were thermally evaporated on ITO substrates with different HTLs sequentially.

4.2. Instruments and Device Characterization. FT-IR spectra were conducted on a Vector 22 FT-IR spectrometer by coating the AHM solution on a KBr crystal and annealing it at different temperatures before measuring. The UV−vis spectra and the transmittance spectra were recorded on SHIMADZU UV-1601PC spectrophotometer. XPS and UPS experiments were performed on a Physical Electronics (PHI) 5600LS electron spectrometer, equipped with a small-spot X-ray source providing monochromatized Al Kα photons (1486.6 eV) for XPS and He I photons (21.2 eV) for UPS, with resolutions of <0.4 and 0.04 eV, respectively. O 1s and Mo 3d high resolution spectra were measured with pass energies of 6 and 3 eV, respectively. The binding energy scale was calibrated by means of an independent Au reference sample, setting the Au $4f_{7/2}$ core level position to 84.00 eV. The surface morphologies of the AHM based HTLs were recorded by AFM (Picoscan PicoSPM LE scanning probe microscope) in tapping mode. The thickness of AHM based HTLs were measured by ellipsometry (GES5, Sopra). The photovoltaic characteristics were measured under a nitrogen atmosphere using a Keithley 2602A source-measure unit and an Abet solar simulator with 100 mW/cm^{2}AM 1.5G illumination, calibrated with an ISE Fraunhofer certified Si photodiode.

■ ASSOCIATED CONTENT

Supporting Information

XPS survey scans of AHM based films, the optical band gaps obtained from the Tauc plot, $J-V$ curves of P3HT/$PC_{60}BM$ devices using H_2O_2 modified AHM HTLs without and with baking, the correlation of H_2O_2 modified AHM HTL thickness to AHM concentration, normalized J_{sc}, V_{oc}, and FF of P3HT/$PC_{60}BM$ conventional structural devices as a function of storage time in air. This material is available free of charge via the Internet at http://pubs.acs.org.

■ AUTHOR INFORMATION

Corresponding Author

*W. Qiu. E-mail: Weiming.Qiu@imec.be.

Notes

The authors declare no competing financial interest.

■ ACKNOWLEDGMENTS

The authors thank Changbo Wu for the FT-IR measurements, David Cheyns for the ellipsometry measurements and Eszter Voroshazi for the useful discussion on the air stability tests of the organic solar cell devices. This project has received funding from the European Union's Seventh Program for research, technological development and demonstration in the frame of ArteSun (grant agreement number: FP7-NMP-2013-SMALL-7/604397).

■ REFERENCES

(1) Brabec, C. J.; Gowrisanker, S.; Halls, J. J. M.; Laird, D.; Jia, S. J.; Williams, S. P. Polymer-Fullerene Bulk-Heterojunction Solar Cells. *Adv. Mater.* **2010**, *22*, 3839−3856.

(2) Li, G.; Zhu, R.; Yang, Y. Polymer Solar Cells. *Nat. Photonics* **2012**, *6*, 153−161.

(3) Rand, B. P.; Genoe, J.; Heremans, P.; Poortmans, J. Solar Cells Utilizing Small Molecular Weight Organic Semiconductors. *Prog. Photovoltaics* **2007**, *15*, 659−676.

(4) You, J. B.; Dou, L. T.; Yoshimura, K.; Kato, T.; Ohya, K.; Moriarty, T.; Emery, K.; Chen, C. C.; Gao, J.; Li, G.; Yang, Y. A Polymer Tandem Solar Cell with 10.6% Power Conversion Efficiency. *Nat. Commun.* **2013**, DOI: 10.1038/ncomms2411.

(5) Hadipour, A.; Cheyns, D.; Heremans, P.; Rand, B. P. Electrode Considerations for the Optical Enhancement of Organic Bulk Heterojunction Solar Cells. *Adv. Energy Mater.* **2011**, *1*, 930−935.

(6) Hadipour, A.; Müller, R.; Heremans, P. Room Temperature Solution-Processed Electron Transport Layer for Organic Solar Cells. *Org. Electron.* **2013**, *14*, 2379−2386.

(7) Ratcliff, E. L.; Zacher, B.; Armstrong, N. R. Selective Interlayers and Contacts in Organic Photovoltaic Cells. *J. Phys. Chem. Lett.* **2011**, *2*, 1337−1350.

(8) Yang, X.; Chueh, C. C.; Li, C. Z.; Yip, H. L.; Yin, P. P.; Chen, H. Z.; Chen, W. C.; Jen, A. K. Y. High-Efficiency Polymer Solar Cells Achieved by Doping Plasmonic Metallic Nanoparticles into Dual Charge Selecting Interfacial Layers to Enhance Light Trapping. *Adv. Energy Mater.* **2013**, *3*, 666−673.

(9) Po, R.; Carbonera, C.; Bernardi, A.; Camaioni, N. The Role of Buffer Layers in Polymer Solar Cells. *Energy Environ. Sci.* **2011**, *4*, 285−310.

(10) Yip, H. L.; Jen, A. K. Y. Recent Advances in Solution-Processed Interfacial Materials for Efficient and Stable Polymer Solar Cells. *Energy Environ. Sci.* **2012**, *5*, 5994−6011.

(11) Suh, Y.; Lu, N.; Lee, S. H.; Chung, W. S.; Kim, K.; Kim, B.; Ko, M. J.; Kim, M. J. Degradation of a Thin Ag Layer Induced by Poly(3,4-ethylenedioxythiophene):Polystyrene Sulfonate in a Transmission Electron Microscopy Specimen of an Inverted Polymer Solar Cell. *ACS Appl. Mater. Interfaces* **2012**, *4*, 5118−5124.

(12) Voroshazi, E.; Verreet, B.; Buri, A.; Muller, R.; Di Nuzzo, D.; Heremans, P. Influence of Cathode Oxidation via the Hole Extraction Layer in Polymer:Fullerene Solar Cells. *Org. Electron.* **2011**, *12*, 736−744.

(13) Steirer, K. X.; Ndione, P. F.; Widjonarko, N. E.; Lloyd, M. T.; Meyer, J.; Ratcliff, E. L.; Kahn, A.; Armstrong, N. R.; Curtis, C. J.; Ginley, D. S.; Berry, J. J.; Olson, D. C. Enhanced Efficiency in Plastic Solar Cells via Energy Matched Solution Processed NiO_x Interlayers. *Adv. Energy Mater.* **2011**, *1*, 813−820.

(14) Chen, S.; Manders, J. R.; Tsang, S. W.; So, F. Metal Oxides for Interface Engineering in Polymer Solar Cells. *J. Mater. Chem.* **2012**, *22*, 24202−24212.

(15) Meyer, J.; Hamwi, S.; Kroger, M.; Kowalsky, W.; Riedl, T.; Kahn, A. Transition Metal Oxides for Organic Electronics: Energetics, Device Physics and Applications. *Adv. Mater.* **2012**, *24*, 5408−5427.

(16) Tan, Z. A.; Li, L. J.; Cui, C. H.; Ding, Y. Q.; Xu, Q.; Li, S. S.; Qian, D. P.; Li, Y. F. Solution-Processed Tungsten Oxide as an Effective Anode Buffer Layer for High-Performance Polymer Solar Cells. *J. Phys. Chem. C* **2012**, *116*, 18626−18632.

(17) Tan, Z. A.; Li, L. J.; Wang, F. Z.; Xu, Q.; Li, S. S.; Sun, G.; Tu, X. H.; Hou, X. L.; Hou, J. H.; Li, Y. F. Solution-Processed Rhenium Oxide: A Versatile Anode Buffer Layer for High Performance Polymer Solar Cells with Enhanced Light Harvest. *Adv. Energy Mater.* **2014**, DOI: 10.1002/aenm.201300884.

(18) Kim, J.; Kim, H.; Kim, G.; Back, H.; Lee, K. Soluble Transition Metal Oxide/Polymeric Acid Composites for Efficient Hole-Transport Layers in Polymer Solar Cells. *ACS Appl. Mater. Interfaces* **2014**, *6*, 951−957.

(19) Manders, J. R.; Tsang, S. W.; Hartel, M. J.; Lai, T. H.; Chen, S.; Amb, C. M.; Reynolds, J. R.; So, F. Solution-Processed Nickel Oxide Hole Transport Layers in High Efficiency Polymer Photovoltaic Cells. *Adv. Funct. Mater.* **2013**, *23*, 2993−3001.

(20) Zilberberg, K.; Trost, S.; Schmidt, H.; Riedl, T. Solution Processed Vanadium Pentoxide as Charge Extraction Layer for Organic Solar Cells. *Adv. Energy Mater.* **2011**, *1*, 377−381.

(21) Tan, Z. A.; Qian, D. P.; Zhang, W. Q.; Li, L. J.; Ding, Y. Q.; Xu, Q.; Wang, F. Z.; Li, Y. F. Efficient and Stable Polymer Solar Cells with Solution-Processed Molybdenum Oxide Interfacial Layer. *J. Mater. Chem. A* **2013**, *1*, 657−664.

(22) Girotto, C.; Voroshazi, E.; Cheyns, D.; Heremans, P.; Rand, B. P. Solution-Processed MoO_3 Thin Films as a Hole-Injection Layer for Organic Solar Cells. *ACS Appl. Mater. Interfaces* **2011**, *3*, 3244−3247.
(23) Yang, T. B.; Wang, M.; Cao, Y.; Huang, F.; Huang, L.; Peng, J. B.; Gong, X.; Cheng, S. Z. D.; Cao, Y. Polymer Solar Cells with a Low-Temperature-Annealed Sol-Gel-Derived MoO_x Film as a Hole Extraction Layer. *Adv. Energy Mater.* **2012**, *2*, 523−527.
(24) Zilberberg, K.; Gharbi, H.; Behrendt, A.; Trost, S.; Riedl, T. Low-Temperature, Solution-Processed MoO_x for Efficient and Stable Organic Solar Cells. *ACS Appl. Mater. Interfaces* **2012**, *4*, 1164−1168.
(25) Jasieniak, J. J.; Seifter, J.; Jo, J.; Mates, T.; Heeger, A. J. A Solution-Processed MoO_x Anode Interlayer for Use within Organic Photovoltaic Devices. *Adv. Funct. Mater.* **2012**, *22*, 2594−2605.
(26) Xie, F. X.; Choy, W. C. H.; Wang, C. D.; Li, X. C.; Zhang, S. Q.; Hou, J. H. Low-Temperature Solution-Processed Hydrogen Molybdenum and Vanadium Bronzes for an Efficient Hole-Transport Layer in Organic Electronics. *Adv. Mater.* **2013**, *25*, 2051−2055.
(27) Zhai, Z.; Huang, X.; Xu, M.; Yuan, J.; Peng, J.; Ma, W. Greatly Reduced Processing Temperature for a Solution-Processed NiO_x Buffer Layer in Polymer Solar Cells. *Adv. Energy Mater.* **2013**, *3*, 1614−1622.
(28) Stubhan, T.; Ameri, T.; Salinas, M.; Krantz, J.; Machui, F.; Halik, M.; Brabec, C. J. High Shunt Resistance in Polymer Solar Cells Comprising a MoO_3 Hole Extraction Layer Processed from Nanoparticle Suspension. *Appl. Phys. Lett.* **2011**, *98*, 253308.
(29) Lee, Y. J.; Yi, J.; Gao, G. F.; Koerner, H.; Park, K.; Wang, J.; Luo, K. Y.; Vaia, R. A.; Hsu, J. W. P. Low-Temperature Solution-Processed Molybdenum Oxide Nanoparticle Hole Transport Layers for Organic Photovoltaic Devices. *Adv. Energy Mater.* **2012**, *2*, 1193−1197.
(30) Meyer, J.; Khalandovsky, R.; Gorrn, P.; Kahn, A. MoO_3 Films Spin-Coated from a Nanoparticle Suspension for Efficient Hole-Injection in Organic Electronics. *Adv. Mater.* **2011**, *23*, 70−73.
(31) Liu, F. M.; Shao, S. Y.; Guo, X. Y.; Zhao, Y.; Xie, Z. Y. Efficient Polymer Photovoltaic Cells Using Solution-Processed MoO_3 as Anode Buffer Layer. *Sol. Energy Mater. Sol. Cells* **2010**, *94*, 842−845.
(32) Murase, S.; Yang, Y. Solution Processed MoO_3 Interfacial Layer for Organic Photovoltaics Prepared by a Facile Synthesis Method. *Adv. Mater.* **2012**, *24*, 2459−2462.
(33) Shao, S.; Liu, J.; Bergqvist, J.; Shi, S.; Veit, C.; Würfel, U.; Xie, Z.; Zhang, F. In Situ Formation of MoO_3 in PEDOT:PSS Matrix: A Facile Way to Produce a Smooth and Less Hygroscopic Hole Transport Layer for Highly Stable Polymer Bulk Heterojunction Solar Cells. *Adv. Energy Mater.* **2013**, *3*, 349−355.
(34) Yao, C.; Xu, X. J.; Wang, J. S.; Shi, L. L.; Li, L. D. Low-Temperature, Solution-Processed Hole Selective Layers for Polymer Solar Cells. *ACS Appl. Mater. Interfaces* **2013**, *5*, 1100−1107.
(35) Hu, X.; Chen, L.; Chen, Y. Universal and Versatile MoO_3-based Hole Transport Layers for Efficient and Stable Polymer Solar Cells. *J. Phys. Chem. C* **2014**, *118*, 9930−9938.
(36) Preparation of Molybdate Solutions, a brochure from climax molybdenum, p 5.
(37) Soultati, A.; Douvas, A. M.; Georgiadou, D. G.; Palilis, L. C.; Bein, T.; Feckl, J. M.; Gardelis, S.; Fakis, M.; Kennou, S.; Falaras, P.; Stergiopoulos, T.; Stathopoulos, N. A.; Davazoglou, D.; Argitis, P.; Vasilopoulo, M. Solution-Processed Hydrogen Molybdenum Bronzes as Highly Conductive Anode Interlayers in Efficient Organic Photovoltaics. *Adv. Energy Mater.* **2014**, DOI: 10.1002/aenm.201300896.
(38) Griffin, J.; Pearson, A. J.; Scarratt, N. W.; Wang, T.; Lidzey, D. G.; Buckley, A. R. Organic Photovoltaic Devices Incorporating a MolybdenumOxide Hole-Extraction Layer Deposited by Spray-Coating from an Ammonium Molybdate Tetrahydrate Precursor. *Org. Electron.* **2014**, *15*, 692−700.
(39) Wienold, J.; Jentoft, R. E.; Ressler, T. Structural Investigation of the Thermal Decomposition of Ammonium Heptamolybdate by In Situ XAFS and XRD. *Eur. J. Inorg. Chem.* **2003**, *6*, 1058−1071.
(40) Buchholz, D. B.; Liu, J.; Marks, T. J.; Zhang, M.; Chang, R. P. H. Control and Characterization of the Structural, Electrical, and Optical Properties of Amorphous Zinc−Indium−Tin Oxide Thin Films. *ACS Appl. Mater. Interfaces* **2009**, *1*, 2147−2153.
(41) Csanyi, L. J. Peroxide Derivatives of Molybdenum(VI) in Acidic Solution. *Transition Met. Chem. (Dordrecht, Neth.)* **1989**, *14*, 298−302.
(42) Moulder, J. F.; Chastain, J.; King, R. C. *Handbook of X-ray Photoelectron Spectroscopy: A Reference Book of Standard Spectra for Identification and Interpretation of XPS Data*; Physical Electronics: Eden Prairie, MN, 1995.
(43) Dupin, J. C.; Gonbeau, D.; Vinatier, P.; Levasseur, A. Systematic XPS Studies of Metal Oxides, Hydroxides and Peroxides. *Phys. Chem. Chem. Phys.* **2000**, *2*, 1319−1324.
(44) Leftheriotis, G.; Papaefthimiou, S.; Yianoulis, P.; Siokou, A.; Kefalas, D. Structural and Electrochemical Properties of Opaque Sol−Gel Deposited WO_3 Layers. *Appl. Surf. Sci.* **2003**, *218*, 276−281.
(45) Braun, S.; Salaneck, W. R.; Fahlman, M. Energy-Level Alignment at Organic/Metal and Organic/Organic Interfaces. *Adv. Mater.* **2009**, *21*, 1450−1472.
(46) Zhou, Y. L.; Holmes, R. J. Influence of a MoO_x Interlayer on the Open-Circuit Voltage in Organic Photovoltaic Cells. *Appl. Phys. Lett.* **2013**, *103*, 053302.
(47) Steirer, K. X.; Chesinc, J. P.; Widjonarko, N. E.; Berry, J. J.; Miedaner, A.; Ginley, D. S.; Olson, D. C. Solution Deposited NiO Thin-Films as Hole Transport Layers in Organic Photovoltaics. *Org. Electron.* **2010**, *11*, 1414−1418.
(48) Tremolet de Villers, B. J.; MacKenzie, R. C. I.; Jasieniak, J. J.; Treat, N. D.; Chabinyc, M. L. Linking Vertical Bulk-Heterojunction Composition and Transient Photocurrent Dynamics in Organic Solar Cells with Solution-Processed MoO_x Contact Layers. *Adv. Energy Mater.* **2013**, DOI: 10.1002/aenm.201301290.
(49) Wong, K. H.; Ananthanarayanan, K.; Luther, J.; Balaya, P. Origin of Hole Selectivity and the Role of Defects in Low-Temperature Solution-Processed Molybdenum Oxide Interfacial Layer for Organic Solar Cells. *J. Phys. Chem. C* **2012**, *116*, 16346−16351.
(50) Wagenpfahl, A.; Rauh, D.; Binder, M.; Deibel, C.; Dyakonov, V. S-Shaped Current-Voltage Characteristics of Organic Solar Devices. *Phys. Rev. B* **2010**, *82*, 115306.